TÜBİTAK

Turkish Journal of Chemistry

http://journals.tubitak.gov.tr/chem/

Research Article

Turk J Chem
(2019) 43: 982 – 993
© TÜBİTAK
doi:10.3906/kim-1812-31

Sensitive biological detection based on Langmuir–Blodgett films prepared from diluted silica suspensions

Numan GÖZÜBENLİ*
Department of Molecular Biology and Genetics, Faculty of Arts and Science, Harran University, Şanlıurfa, Turkey

Received: 19.12.2018 • **Accepted/Published Online:** 08.05.2019 • **Final Version:** 11.06.2019

Abstract: Self-assembled three-dimensional (3-D) colloidal crystals have been extensively utilized in nanolithography for fabricating a wide spectrum of functional periodic nanostructures for important technological applications. Here a simple and versatile way is reported using silica colloids to prepare close-packed particle multilayers by the Langmuir–Blodgett technique to create highly ordered 3-D colloidal crystals with unusual nanoarrays on a large variety of substrates. Successive deposition of monolayers using amphiphilic molecules in this approach allows control of the layer thickness, particle size, and especially packing structure of them in each layer. It has been demonstrated that the Langmuir–Blodgett film's transparency and high antiglare optical properties are preserved even after multiple colloidal particle transfers on both straight and curved surfaces. The surface prepared by the Langmuir–Blodgett technique shows remarkable sensitivity for potential biodetection applications. These colloidal templated films have an optical response time of less than 40 s against essential bioproduct vapors. It is shown that the results are consistent with the Kelvin equation ($\ln P/P_o = -2\ Vl\ \gamma/rRT$) when the liquid water layer is getting thicker.

Key words: Langmuir–Blodgett, nanobiosensor, nanolithography, close-packed silica colloids, porous film, biodetection

1. Introduction

Currently, self-assembled colloidal arrays are preferred for their extensive potential technology applications, for example as structural templates in the production of moth-eye antireflection coatings [1–3]. Layer-by-layer (LbL) assembly, polyelectrolytes, and dip-coating techniques accomplish high quality antiglare coatings on nonflat surfaces [4,5]. The bottom-up techniques, like LbL assembly, and dip-coating based on multiple steps, are limited to single-side coatings on planar substrates; unfortunately, two distinct antireflection surfaces cannot be coated at the same time using these kinds of techniques. Studies on reflection loss in incoming light onto an optical surface in solar panels or optic sensors may also contribute to the development of optical sensitivities. As is known, a typical untreated glass refractive index is 1.5. This refractive index difference between air and glass means a loss of about 10% of incoming light intensity. The low performance of optical systems and readability problems caused by reflection on screens can be improved with multiple optical components [6,7]. Antireflective coatings are one of these components, which are widely used in optical sensors to reduce light reflection and enhance optical transmission [8]. These coatings based on both top-down and bottom-up techniques at visible wavelengths can reduce light reflection over a wide wavelength range and incidence angles [9]. However, the costs of these coatings against reflection are high as they require high vacuum conditions. A wide variety of optical transmission technologies based on dilute suspension processing can provide a simple and more economical

*Correspondence: gnuman@harran.edu.tr

method [10]. Microporous films formed by the phase removing of polymer matrix, self-assembling of nanobeads and polyelectrolyte multiple layers, and many other approaches have been already used in the production of optical coatings on various substrates [11,12].

Microporous films, such as 2-D titanium photonic crystals, are widely used in the detection of volatile components. The concentration of condensation can be monitored in proportion to the change in the optical properties of the diffraction medium during condensation (e.g., the wavelength shift of the photonic band cavities or interferometry). Nanolithography including self-assembly techniques has been successful in the creation of photonic structures for chemical and biological detection. The mechanisms of color production in the present nanofabricated photonic sensing materials include localized plasmon resonance, Bragg diffraction, and Fabry–Perot interferometry. One advantage of these photonic structures on organic dyes is elimination of photobleaching problems. Unfortunately, the main limitations of the current nanophotonic sensor materials are their high cost, small-scale productivity, and low response selectivity to different analyses.

The Langmuir–Blodgett (LB) coating technique, which uses amphiphilic molecules spread at the interface between water and air, might be an important candidate to handle these limitations. A series of monolayers are deposited one by one on the surface to be coated. The physical conditions used for the crystallographic structure of films and their effects on the coating technique are discussed. LB films prepared using various particle sizes were examined for ideal optical detection. The physical details and the possible technical applications in the sensing studies are explained herein. The methods followed while preparing these 3-D colloidal films and practical solutions are given. 3-D highly ordered LB crystal films based on close-packed (cp) templates (or colloidal particles) are very similar to microarrays on blue morpho butterfly wings used in highly selective component detection [13]. Therefore, 3-D microporous polymer photonic crystals formed by a cheap and scalable bottom-up technology make it possible to detect a wide variety of vapors reproducibly. Capillary condensation measurements in submicrometer-scale structures have been investigated with both experiments and theoretical calculations [14–17]. The reflection spectra of the scales provide information about the structure and concentration of the vapors, allowing the identification of a closely related series of isomers of ethanol, and acetic acid when analyzed individually. Nanotechnology tries to mimic partial photonic band-gap structure and irradiation of the morpho butterfly scale with new visual effects and functions [18]. However, exact combination of its 3-D structure and cuticle complex refractive index is still beyond the nanofabrication capabilities. For solutions to be improved by bioengineering technologies to the challenges we face in everyday life, it is certain that nature has a lot to teach us.

2. Materials and methods

A two-step colloidal self-assembly technique that performs deposition of two colloidal layers on both sides of a glass substrate was examined. The first part of this study is about polymer structured nanoporous films with 3-D hexagonal arrays of voids obtained by LB coating technique examined in previous studies [19,20]. To prepare these porous films showing plasmonic features, silica microspheres washed in 200-proof ethanol at least 4 times are dispersed in ethylene glycol ($C_2O_2H_6$) with a particle volume fraction of 0.20. The most stringent cleaning procedures must be followed in the LB work. The beaker and its accessories for the LB coating process are required to be free of surface-active materials and greases. The glassware must be washed with oxidants and rinsed with plenty of ultrapure water. To avoid any residues being left on the cleaned surface, reagent quality solvents must be used. Moreover, very high purity water must be used, and preferably for each new monolayer spread it should be changed at intervals to avoid bacterial growth in water left in the

beaker. Ultrapure water is usually supplied by the existing purification systems including ultrafiltration and ion exchange techniques. Small nonionizable impurities may still affect the behavior of particle crystallization although these filtration systems are provided with a resistivity meter allowing continuous assessment of the quality of the water. Monodispersed silica particles with diameter of 100, 200, and 600 nm and size distribution of less than 6% were synthesized by following the standard Stober method. After at least 4 redispersion cycles in ethanol for purification, colloidal suspensions were entirely dispersive in ethylene glycol upon operating 20 kHz applied by a probe Q700 sonicator. After the silica/ethylene glycol suspension was prepared, it was added dropwise slowly to the deionized water surface in a clean beaker as shown in Figure 1. For the preparation of a polymer membrane film based on ETPTA monomer cast on self-assembled layers coated on glass, the photo initiator was mixed with the monomer, in which 1% (weight) ratio of Darocur 1173 was used to polymerize the monomer. ETPTA monomer was photopolymerized for 4 s using a pulsed UV curing system (RC 742, Xenon). Before the glass microslides were coated, they were immersed in nitric acid/sulfuric acid mix in equal volumes (1:1) on a hot plate at 120 °C for 20 min. After completing the first transfer of spheres onto the glass surface, the second transfer was carried out by following the same track. After each transfer, ETPTA monomer as a nonvolatile monomer is cast on the monolayers to get the main backbone of the porous film. The coated silica nanospheres can then be completely removed by etching in a 2 vol % hydrofluoric acid aqueous solution at least 20 min. After cleaning with ethanol and drying with air blow pump, the self-assembled nanoporous polymer films will have uniform and shining colors. In the second part of the study, these porous films based on a template of photonic crystals, which demonstrate uniform and shining colors as result of Bragg diffraction of visible light from 3-D highly ordered air cavities, can thus be designated for vapor detection.

2.1. Chemical reagents

All solvents and chemicals used in this study were of reagent quality and no further purification was required. The 200-proof ethanol was purchased from Pharmaco Products. Ethoxylated trimethylolpropane triacrylate

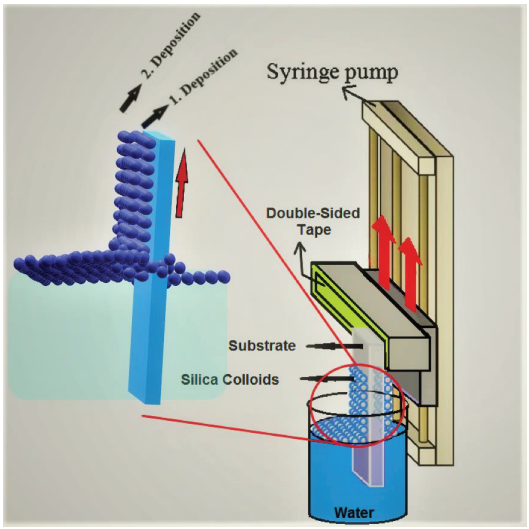

Figure 1. Schematic representation of cp colloidal crystals that can be coated on glass with the Langmuir–Blodgett technique (see left inset). The colloidal self-assembly process for colloids on both sides of a substrate in two steps is implemented. Apart from the washing of the glass surface in previously prepared gold water, multiple transfers of the ordered silica particles of 100, 200, and 600 nm were carried out without APTCS and an additional oxygen plasma etching process.

monomer (ETPTA, SR 454) was obtained from Sartomer. Norland Optical Adhesive 60, known as mercapto-ester (alkyl urethane), was ordered from Norland Products Incorporated. Photo initiator, Darocur 1173 (2-hydroxy-2-methyl-1-phenyl-1-propanone), was provided by Ciba-Geigy. Glass microslides (75 mm × 25 mm) were purchased from Thermo Fisher Scientific.

2.2. Instrumentation

Scanning electron microscopy images were taken using a Zeiss-SEM Evo50. The syringe pump (KD Scientific 780-230) was purchased from Thermo Fisher Scientific. A thin layer of gold (roughly thickness of 2-3 nm) was sputtered onto the samples prior to imaging. A pulsed UV curing system (RC 742, Xenon) was used to polymerize the ETPTA monomer. The specular reflectance was obtained using an Ocean Optics HR4000 UV-vis spectrometer.

2.3. Transfer of monolayer of cp silica colloids onto glass slides

A monolayer of silica particles on the deionized water surface was transferred to glass slides (75 mm × 25 mm) using double-sided tape attached to the syringe pump. The glass slides were cleaned by immersing in nitric acid/sulfuric acid mix in equal volumes (1:1) on a hot plate at 120 °C for 20 min, and then rinsed with pure EtOH twice. The silica monolayer transferred to the glass slides was placed vertically and left to dry for 10–15 min. After the first transfer of silica particles from the deionized water surface to the glass slides and following ETPTA monomer coating, the second transfer from the water surface was performed by a similar method. LB coating-based colloidal transfers were accomplished repeatedly for different size particles in the same procedure.

3. Results and discussion

The colloidal self-assembly technique based on LB coating can be used to improve biosensor surfaces even on a scalable curved surface from the glass slide because of strong capillary interactions among colloidal beads on the water surface. An example of the LB technique was set up as seen in Figure 1. Due to the strong surface tension of the water (72.60 mN/m at 22 °C) and the strong capillary action among the silica particle spheres, the iridescent colors caused by the light diffraction are observed on the water and colloidal crystal monolayers are assembled as depicted in Figure 1. It is seen that cp colloidal crystals are coated on the glass by the LB technique. The colloidal self-assembly process for two layers on both sides of a substrate in two steps is depicted. Except for washing of the glass surface with preprepared gold water, multiple transfers of the silica particles of 100, 200, and 600 nm were achieved without APTCS, which is a kind of optic glue, and an oxygen plasma etching process. A vertical beveled syringe pump arm pulls the glass slide with a uniform capillary force to align silica microspheres on the glass surface. The glass slide vertically immersed is moved at a controlled speed (refer to schematic illustration in Figure 1). The silica/ethylene glycol suspension was added a few drops per minute onto the surface of deionized water. Silica nanospheres were floated at the water–air interface, which resulted in an iridescent colloidal crystal film on the surface of the water. ETPTA polymer as the backbone of the porous film on the glass surface to support the porous film is chemically bonded on the glass substrate surface. It is also clear from these SEM images that the cp structure of monolayer colloidal particles is crystallized hexagonally. A periodic monolayer embedded in ETPTA polymer is clearly seen on the copolymer surface. The hexagonal Bragg diffraction pattern on the copolymer, following the second LB transfer process and ETPTA coating, is well retained (see Figures 2A, 2B, and 2C). Side-tilted top pictures of glass slides in Figures 2A, 2B, and 2C are given for their distinct color reflections, which are visible to the naked eye. The color variations in

the close-packed colloidal film samples in Figures 2A–2C are the result of this iridescence effect that depends on the particle size and crystal orientation. The colloidal film surfaces colored differently in Figures 2A–2C prove that the wavelength of color is related to particle size. As the particle size increases, the diffraction of incoming light from the colloidal multilayer film surface passes into the visible region and the resulting colors are from light to dark blue. The copolymer matrix with silica crystals on the glass slide becomes more purplish at the same viewing angle. The yellow, greenish, and bluish colors obtained by diffractions on the films seen in Figures 2A, 2B, and 2C, respectively, are compatible with wavelength shifts depending on the high spherical hexagonal template sizes. The spreading colloidal suspension takes almost 5 min to cover the whole surface area of a beaker. An immersed glass microslide in water was withdrawn vertically by a KD Scientific 780-230 syringe pump at a rate of ∼20 mm/min. Each side of the glass substrate was evenly coated with highly uniform colloidal particles.

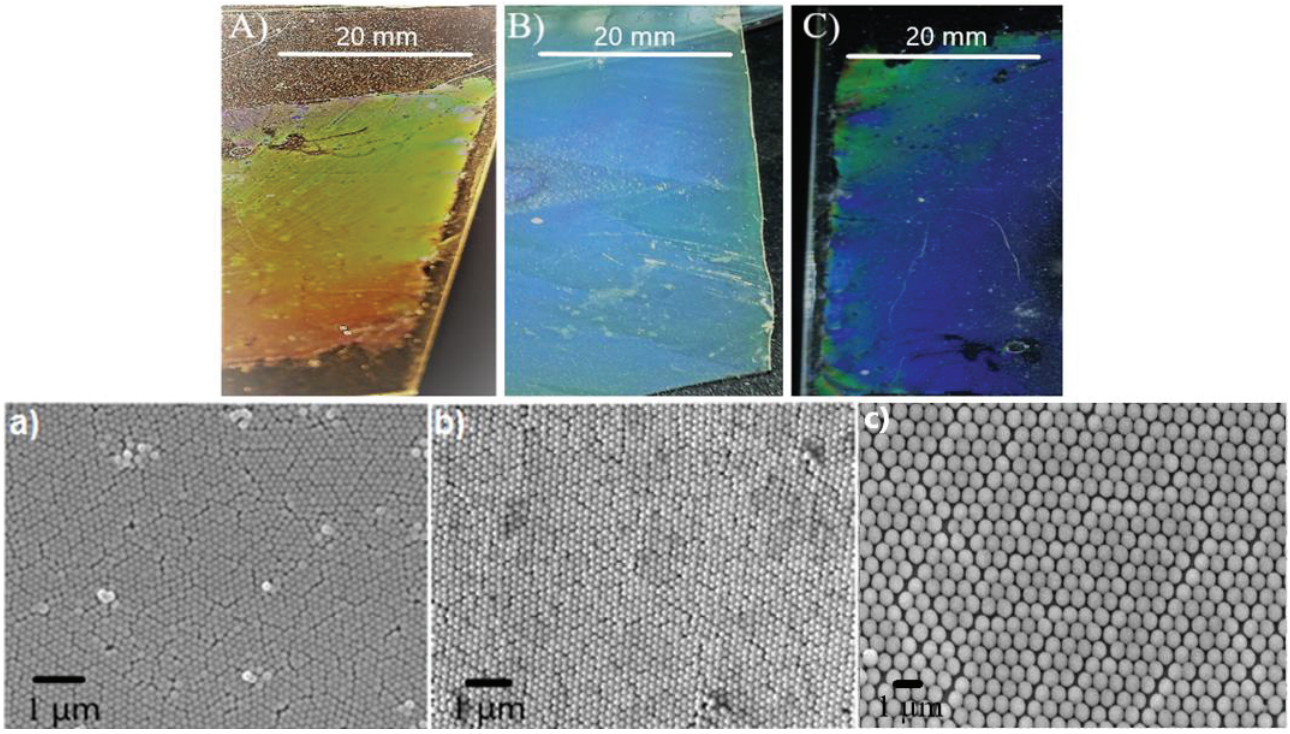

Figure 2. The color variations in the close-packed colloidal films (top row; A, B, C) are a result of the iridescence effect that depends on the particle size. The close-packed colloidal layer of (a) 100 nm, (b) 200 nm, and (c) 600 nm silica spheres are given by top-view SEM images. Hexagonal silica crystal arrays with diameter of 100, 200, and 600 nm after EtOH washing of a 2-in. sized glass coated by Langmuir–Blodgett coating in ethylene glycol with particle volume fraction of 0.20.

3.1. Surface imaging

The surface of the colloidal self-assembled film and its porous structure were lightened by a Zeiss-SEM Evo50 microscope at a power setting of 15.0 kV. SEM images of highly structured colloidal films covered with 5 nm of Au/Pd as a conductive layer were obtained and no extra pretreatments were carried out for only the images in Figures 2a– 2c. The purpose of this conductive layer of metal on the sample is to inhibit charging, reduce thermal damage, and improve the secondary electron signal required for topographic examination in the SEM. A

hexagonal monolayer of the self-assembling colloidal particles was revealed by SEM images. Other SEM images were taken for multilayer porous films and were obtained by removal of colloidal particles by acidic etching prior to optical measurements. Top-view SEM images of colloidal particles on the left half of the glass slide in Figures 2a–2c covered by a transferred layer of 100, 200, and 600 nm silica spheres are shown, respectively.

Additionally, the size of self-assembled particles is simply determined by SEM ruler. After treatment of silica particles with diluted HF acid solution for 30 min, all colloidal particles were removed. However, the prepared 3-D nanoporous films still have iridescent yellow, greenish, and bluish colors based on Bragg diffraction of visible light caused by hexagonal orders of colloids. The number and thickness of the layers of silica colloidal multilayer films were determined by SEM images. The hexagonal array of cp particles embedded in ETPTA copolymer on the glass slide was confirmed by the top- and side-view SEM images given in Figures 3a–3c, respectively. From detailed top-view and cross-sectional SEM images, it was proved that the assembled colloidal crystals on the glass slide are double layers. The porous polymer template is shown (the inset: top view) after removing the silica colloids from the porous ETPTA backbone. More details about the double layers formed can be found in the inset after LB transfers and HF treatment. The double layer prepared by the LB coating process has a highly ordered hexagonal structure composed of hexagonally ordered composite crystals on the glass surface. The silica particles' templates (the inset) make large air cavities interconnected through contact points, which originate from the close-packed silica microspheres in the capillary force-aligned layer. Some defects such as agglomeration or crystal unit boundaries might be apparent, but hexagonal arrays based on close-packed silica nanoparticles can be obviously selected. Because many of these intrinsic defects are subwavelength scale, they do not have a significant effect on the optical detection or Bragg diffractions. The crystalline domain size is the size of the deionized water surface, and the surface coating process will be an ongoing process if the suspension concentration is kept constant. The capillary interactions among colloidal particles, which are the major driving force for the observed colloid particle crystallization, increase proportional to the size of the colloidal spheres [21].

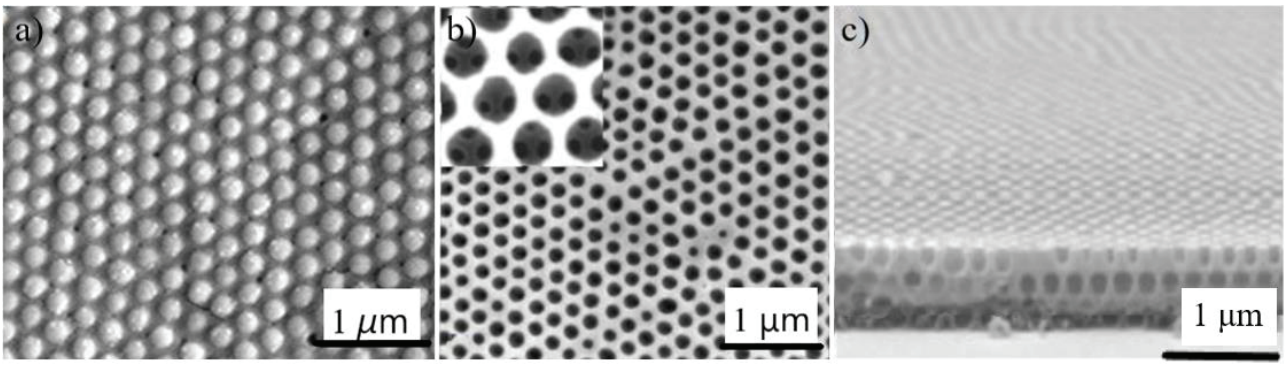

Figure 3. SEM images of colloidal crystals comprise (a) top-view monolayer before HF acid etching treatment, and (b) double layer after HF acid etching treatment (inset: the appearance of two layer from the voids). Membrane porous film is prepared after immersing it in a 2 vol. % hydrofluoric acid aqueous solution for 30 min, (c) side view of membrane layer based on hexagonal cp 200 nm colloidal particles obtained via the Langmuir–Blodgett technique.

The hexagonally arranged spheres within each colloidal layer are in contact with each other, which will create voids in the main backbone of the porous film. Adjusting coating conditions based on the syringe pump such as speed, time, and concentration of suspension can exactly control the thickness of capillary force-aligned particles on the wafer [22]. Capillary force-aligned colloidal particles are highly embedded in the polymer matrix,

which has a highly uniform thickness on the area of the glass slide. Silica particles embedded in the copolymer based on ETPTA monomer can be transferred and then used on any surface using optical glues. Besides ethylene glycol surfactant used on DIY water during the LB coating process, the only ETPTA monomer might be applied to get highly ordered arrays and templates. They can be fabricated as molds for soft lithography [23–25] and nanoimprint lithography [26,27] to produce highly uniform nanodots and nanohole arrays.

3.2. Optical characterization

A HR4000 NIR512 Vis-NIR spectrometer (Ocean Optics) with a reflection probe as a gas detector was used to carry out the optical reflection and spectral peak position measurements of the self-assembled nanoporous film. For optical illumination, a calibrated tungsten halogen light source was used. The probe beam size on the sample surface is about 3 mm. Optical measurements from the Vis-NIR spectrometer were performed by applying normal incidence. The cone angle of collection is less than 5 degrees. Absolute reflectivity was calculated as a ratio of the sample spectrum and the reference spectrum. The absolute refractive index is often referred to for distinguishing it from definitions where the speed of light in other reference media (a silicon wafer in this study) than a vacuum is used. An aluminum-sputtered (1000 nm thickness) silicon wafer was used to determine the reference spectrum to measure optical density. Ten different spots obtained from the sample surface were accepted as the final average value of absolute reflectivity. In the present study, it was aimed that optical reflection would be efficiently improved if the difference between the refractive index of the coating and the geometric mean of the refractive indices of the two media at the interface increased.

3.3. Optimal design and analysis of the sensor

The optical performance of the sensor was examined by establishing an optical gas detection system. Electrical feeds for the thermocouple were made along the lower plate of the gas chamber as shown in Figure 4. The film surface on the glass substrate was checked up to the required operating temperatures to reach a constant temperature. The incoming light passing through the probe element and then diffracted light from glass substrate were monitored using a relay with adjustable time intervals. A platinum thermocouple was used to ensure a stable operating temperature of the sensor. The thermocouple has digital temperature indicators, and one port connected to the N_2 gas inlet was used as a vapor inlet valve in Figure 4. The required partial pressures of the gas mixture inside the static system were calculated by injecting a known volume of test vapor. A constant incoming light intensity was applied to the film surface, and absolute reflectivity was measured by a Vis-NIR spectrometer. The moisture-free pure air was allowed to pass into the polyurethane gas chamber after the gas mixture exposure cycle as shown in Figure 4. The prepared porous 3-D polymer film (bluish surface on right) was tested in a gas chamber for optical measurements as illustrated in Figure 4. After the polyurethane gas chamber was discharged by pure air, depending on the partial pressure to be applied, the gas composed of a mixture of analyte vapor and nitrogen gas was loaded. Total pressure of the chamber was controlled by pure nitrogen gas to be 1 atm. The normal specular reflectance spectra come from a nanoporous ETPTA film including 200 nm air cavities in ethanol vapors with different partial pressures (from 0 P_0 to 1.0 P_0) at 56 $\pm$ 1 °C. P_0 at this temperature is known as the saturation vapor pressure of ethanol (280 mmHg). The obtained spectra are evidence of different Bragg diffractions with Fabry–Perot parallel beam lines showing high quality photonic crystal properties combined with the LB coating technique. The comparison was not shown between deposited and bare glass in the figures because no shifts or signals at specific wavelengths for various glass surfaces (not coated) were observed in the range of visible light [26,27]. Specific signals in

wavelengths and linear shifts in wavelengths corresponding to partial pressure are important indicators in the selection of nanoporous film as a sensor surface for vapor detection. When ethanol partial pressure in vapor is increased, ethanol condensation in the inner surfaces of the void of the film leads to an effective refractive index of the diffractive medium and a smaller dielectric contrast among polymer void templates. Figure 5A compares the specular reflection spectra obtained at normal incidence from the bare glass substrate by applying different partial pressures of ethanol vapors. The observed red wavelength-shift of the Bragg diffraction peaks and the reduction of the amplitude of the optical stop bands (as shown in Figure 5A) can be associated with this situation. The shift of diffraction peaks can be assumed to be almost linear relating to the ethanol partial pressure in Figure 5B. When the ethanol vapor is removed, the prepared 3-D films and their optical properties are completely recovered. Therefore, multilayer colloidal template films can provide a sustainable way for distinct practices of vapor detection many times. To make an evaluation of the speed of response of the colloidal template vapor detector, a diagram is given in Figure 6 that measures the average optical response time taken from different spots on the sample surface in ethanol vapor. In Figure 6A, the spectral peak positions obtained from the surface of the nanoporous polymer film in ethanol vapor and their time dependence are given at a constant partial pressure ($0.5\ P_0$) and temperature ($56\ ^\circ C$). The spectral peak positions and the optical response time (in Figures 6A and 6B) were also found by using the same spectrometer in addition to optical reflection measurements. According to Figures 6A and 6B, surface response time and vapor pressure balance are observed to be achieved in less than 1 min. In Figure 6B the curve represents the response time following an abrupt positive going step-function change as an output from Bragg diffraction. The wavelength of the Bragg diffraction of the incoming light reaches an output peak against the ethanol vapor exposure time. The time required for detection, such as the adsorption of alcohol vapor on the film surface and the balance of surface interactions, is defined as the T_D delay time in Figure 6B. It will be seen that the prepared 3-D film has an optical response time of less than 40 s against ethanol vapor. The response time for detection of biological components can be explained by ethanol's volatile chemical structure and high viscosity. However, the response time is the same for acetic acid. Therefore, the optical response time of the detection surface in this regard proves that it is not connected with the type of chemical analyte. It is assumed that colloidal nanoparticles under the influence of capillary forces were hexagonally close-packed on both surfaces of a glass substrate because of the principle of minimum energy requirement for the self-assembly process. It is obvious that the spectra's shifts are compatible with the changes in analyte concentrations regarding the shape and peak position of the reflection spectra.

When the same conditions (i.e. vapor partial pressures and temperatures) can be applied in essential fatty acids, which exhibit vapor at certain temperature and pressure values, it is estimated that a similar response time can be achieved in essential fatty acids. For this reason, biological metabolism and diagnostic studies for essential fatty acids will be among the priorities of our future studies. To make the nanoporous photonic film-based vapor detector more understandable, the amount of liquid ethanol on the porous internal surface of film at different partial pressures can be calculated by the Kelvin equation [28–31]. Surface structures, their positions, the displacement toward the red end of the spectrum wavelength, and broad diffractive peaks associated with the condensation of ethanol vapor in the voids agree well with the experiments, although the experimental results have lower reflectance compared to the simulated spectra. In nanoporous photonic crystals, we can say that ethanol vapor is concentrated by capillary action at certain temperatures and pressures. In the Kelvin equation, $\ln P/P_o = -2\ V_l\gamma/rRT$, γ: the liquid surface tension, V_l: the liquid molar volume, r: the radius of curvature, P, and P_0: actual, saturation vapor pressure, respectively. Capillary condensation can

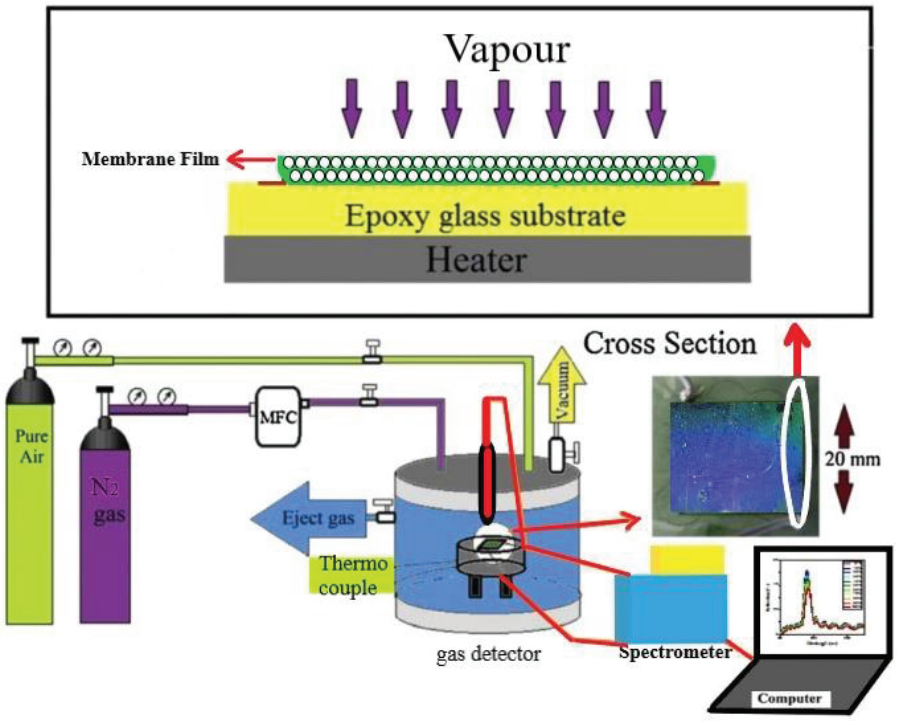

Figure 4. Schematic representation of the biodetector used to detect volatile biological components. a) Cross section of membrane film composed of 200 nm templates of colloidal particles in the top box, and top view of 20 mm membrane film under the box. b) The volatile component analysis chamber consists of a spectrometer that reads the diffraction wavelength shift values of a component on the membrane film at a constant temperature and a partial pressure in a vacuum environment and a computer connected to it.

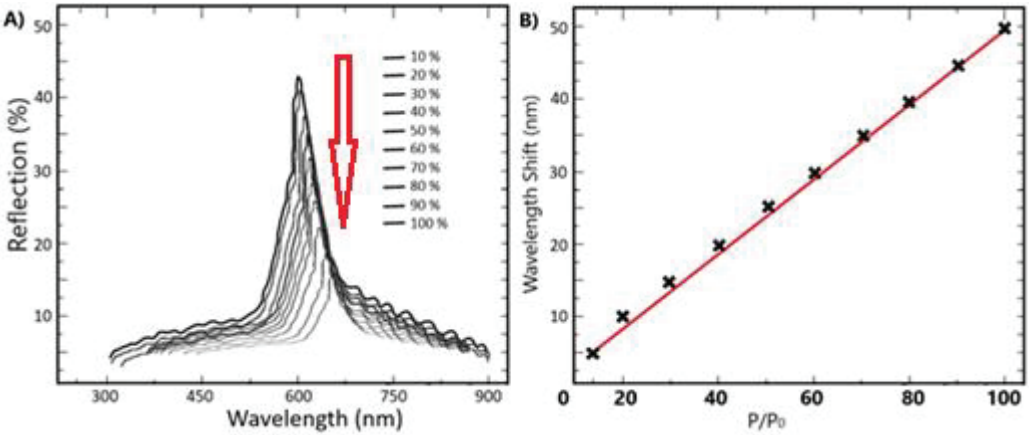

Figure 5. A) Normal frequency specular reflection spectra by applying different partial pressures of ethanol vapors to a 200 nm porous polymer film. While the wavelength of the analyte is proportional to the vapor partial pressure, the reflection decreases with partial pressure. B) Wavelength shift values against the partial vapor pressure of the Bragg diffraction peak.

be explained by this equation because the nanoporous film contains spherical meniscus voids. The radius of liquid film curvature adsorbed on the nanoporous film is inversely proportional to the radius of the air cavity. Therefore, if a higher vapor partial pressure is applied, it results in a thicker liquid layer, which means a smaller

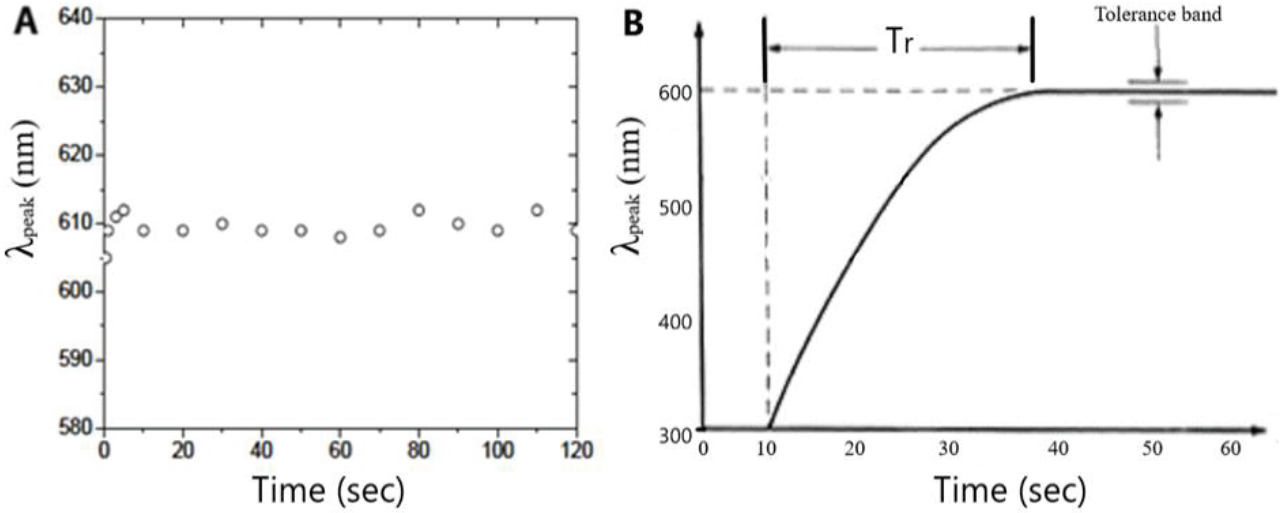

Figure 6. A) The spectral peak positions obtained from the surface of nanoporous polymer film in ethanol vapor and their time dependence are given at a constant partial pressure. B) The optical response time of 3-D nanoporous film to the incoming light in ethanol vapor is measured.

r. If all constants (i.e. γ, Vl, R, and T) are fixed, P is proportional to r. The wavelength shifts obtained from ethanol and acetic acid vapors demonstrate that this is compatible with the experimental results when the liquid water layer is getting thicker. The thin liquid layer condensed at low partial pressures may not show steady-state process features. For this reason, the small deviations in the different data points in Figure 7A and 7B can be explained by this thin liquid layer. Vapor detection based on the nanoporous film can be readily applied to a large variety of vapors, for example acetic acid and essential (volatile) fatty acids. Acetic acid detection has almost the same process as ethanol detection as seen in the figures. Briefly, in the present study, the surface of nanoscale voids is covered by water vapor that creates a liquid layer on the inner surface of pores [32–34]. Nanoporous films prepared by a continuous and reproducible LB technique have been shown to be able to be used for vapor detection.

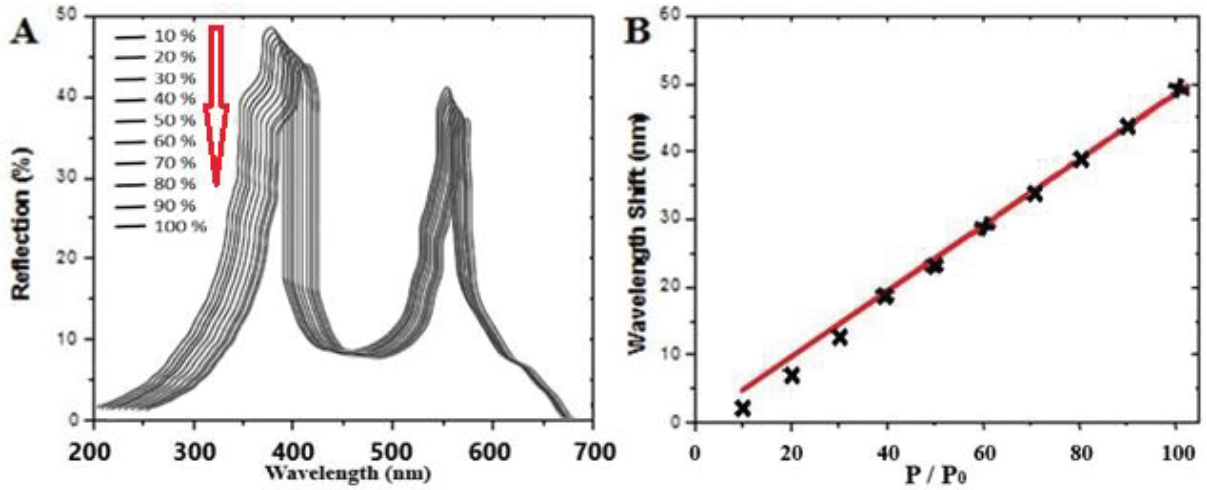

Figure 7. A) Normal visible specular reflection spectra by applying different partial pressures of acetic acid vapors to a 200 nm porous polymer film. B) Wavelength shift values against acetic acid partial vapor pressures of the Bragg diffraction peak.

3.4. Conclusions

It is shown that a highly ordered close-packed colloidal porous film on a variety of technologically important substrates can be used to detect critic biological reactants such as acetic acid, uric acid, ethyl alcohol, and ketone compounds, which are important for biological metabolism. A porous detection film composed of two layers at different levels of the same crystal structure can be achieved by adjusting syringe pump conditions and the size of particles used in colloidal suspension with only acid etching. This method, which is sustainable for self-assembly of nanoarrays by multitransfer, can also lead to sudden developments that will be utilized in future for potential technology applications. Several advantages over previous self-assembly techniques are seen with the LB technique used here. Firstly, it is scalable and has high reproducibility. A steady-state operation based on LB coating can be practically performed in minutes, while classical methods take even weeks to produce a meter-size nanocolloidal film. Optical properties of LB films like transparency and high antiglare are present even after multitransfer of colloidal particles on both flat and curved surfaces, which are not easily available by current top-down and bottom-up approaches. The LB coating technique can be a new candidate for scalable production of periodic nanostructured films that have applications ranging from sensitive biosensors to smart drug design.

Acknowledgment

This research was supported by grants from Harran University.

References

1. Askar K, Phillips BM, Fang Y, Choi B, Gozubenli N et al. Self-assembled self-cleaning broadband anti-reflection coatings. Colloids and Surfaces a-Physicochemical and Engineering Aspects 2013; 439: 84-100.
2. Askar K, Gu Z, Leverant CJ, Wang J, Kim C et al. Self-assembled nanoparticle antireflection coatings on geometrically complex optical surfaces. Optics Letters 2018; 43: 5238-5241.
3. Jiang P, Prasad T, McFarland MJ, Colvin VL. Two-dimensional nonclose-packed colloidal crystals formed by spincoating. Applied Physics Letters 2006; 89: 1.
4. Jiang P, McFarland MJ. Large-scale fabrication of wafer-size colloidal crystals, macroporous polymers and nanocomposites by spin-coating. Journal of the American Chemical Society 2004; 126: 13778-13786.
5. Jiang H, Yu K, Wang, Y. Antireflective structures via spin casting of polymer latex. Optics Letters 2007; 32: 575-577.
6. Liu X, Choi B, Gozubenli N, Jiang P. Periodic arrays of metal nanorings and nanocrescents fabricated by a scalable colloidal templating approach. Journal of Colloid and Interface Science 2013; 409: 52-58.
7. Nakashima A, Edamatu M, Kushi K. Dip-coating method. Google Patents: 1982.
8. Yang H, Gozubenli N, Fang Y, Jiang P. Generalized fabrication of monolayer nonclose-packed colloidal crystals with tunable lattice spacing. Langmuir 2013; 29: 7674-7681.
9. Hiller J, Mendelsohn J D, Rubner MF. Reversibly erasable nanoporous anti-reflection coatings from polyelectrolyte multilayers. Nature Materials 2002; 1: 59-63.
10. Yang JC, Gao H, Suh JY, Zhou W, Lee MH et al. Enhanced optical transmission mediated by localized plasmons in anisotropic, three-dimensional nanohole arrays. Nano Letters 2010; 10: 3173-3178.
11. Zhao Y, Wang J, Mao G. Colloidal subwavelength nanostructures for antireflection optical coatings. Optics Letters 2005; 30: 1885-1887.
12. Walheim S, Schaffer M, Mlynek S, Steiner U. Nanophase-separated polymer films as high-performance antireflection coatings. Science 1999; 1095-9203(Electronic).

13. Bardosova M, Pemble ME, Povey IM, Tredgold RH. The Langmuir-Blodgett approach to making colloidal photonic crystals from silica spheres. Advanced Materials 2010; 22: 3104-3124.
14. Dague E, Jauvert E, Laplatine L, Viallet B, Thibault C et al. Assembly of live micro-organisms on microstructured PDMS stamps by convective/capillary deposition for AFM bio-experiments. Nanotechnology 2011; 22.
15. Grzybowski BA, Bowden N, Arias F, Yang H, Whitesides GM. Modeling of menisci and capillary forces from the millimeter to the micrometer size range. Journal of Physical Chemistry B 2001; 105: 404-412.
16. Kim S, Jung JW, Lee TS, Jeong JH, Lee SY et al. Large area asymmetric ferromagnetic nanoring arrays fabricated by capillary force lithography. Electronic Materials Letters 2012; 8: 71-74.
17. Kralchevsky P, Denkov N, Paunov V, Velev O, Ivanov I et al. Formation of two-dimensional colloid crystals in liquid films under the action of capillary forces. Journal of Physics: Condensed Matter 1994; 6: A395.
18. Jiang P. Large-scale fabrication of periodic nanostructured materials by using hexagonal non-close-packed colloidal crystals as templates. Langmuir 2006; 22: 3955-3958.
19. Stober W, Fink A, Bohn E. Controlled growth of monodisperse silica spheres in the micron size range. Journal of Colloidal Interface Science 1968; 26: 62.
20. Yang H, Jiang P. Large-scale colloidal self-assembly by doctor blade coating. Langmuir 2010; 26: 13173-13182.
21. Jiang P, McFarland MJ. Wafer-scale periodic nanohole arrays templated from two-dimensional nonclose-packed colloidal crystals. Journal of the American Chemical Society 2005; 127: 3710-3711.
22. Huang WH, Sun CH, Min WL, Jiang P, Jiang B. Templated fabrication of periodic binary nanostructures. The Journal of Physical Chemistry C 2008; 112: 17586-17591.
23. Middleman S. The effect of induced air-flow on the spin coating of viscous liquids. Journal of Applied Physics 1987; 62.
24. Xia Y, Walgree GM. Soft lithography. Angewandte Chemie International Edition 1998; 37: 550-575.
25. Bowden N, Choi IS, Grzybowski BA, Whitesides GM. Mesoscale self-assembly of hexagonal plates using lateral capillary forces: synthesis using the "capillary bond". Journal of the American Chemical Society 1999; 121: 5373-5391.
26. Park HJ, Kang MG, Guo LJ. Large area high density sub-20 nm SiO_2 nanostructures fabricated by block copolymer template for nanoimprint lithography. ACS Nano 2009; 3: 2601-2608.
27. Jung WK, Kim NH, Byun KM. Development of a large-area plasmonic sensor substrate with dielectric subwavelength gratings using nanoimprint lithography. Journal of Biomedical Nanotechnology 2013; 9: 685-688.
28. Bird SA, Jajam KC, Tippur HV, Auad ML. Synthesis and characterization of high performance, transparent interpenetrating polymer networks with polyurethane and poly(methyl methacrylate). Polymer Engineering and Science 2013; 716-723.
29. Baley C. Analysis of the flax fibres tensile behaviour and analysis of the tensile stiffness increase. Composites Part A: Applied Science and Manufacturing 2002; 33: 939-948.
30. Sun ZQ, Li Y, Zhang JH, Li YF, Zhao ZH et al. A universal approach to fabricate various nanoring arrays based on a colloidal-crystal-assisted-lithography strategy. Advanced Functional Materials 2008; 18: 4036-4042.
31. Sun CH, Gonzalez A, Linn NC, Jiang P, Jiang B. Templated biomimetic multifunctional coatings. Applied Physics Letters 2008; 92: 051107.
32. Jiang P, Bertone J, Hwang K, Colvin V. Single-crystal colloidal multilayers of controlled thickness. Chemistry of Materials 1999; 11: 2132-2140.
33. Sun CH, Jiang P, Jiang Bin. Broadband moth-eye antireflection coatings on silicon. Applied Physics Letters 2008; 92: 61112.
34. Suh JY, Huntington MD, Kim CH, Zhou W, Wasielewski MR et al. Extraordinary nonlinear absorption in 3D bowtie nanoantennas. Nano Letters 2012; 12: 269-274.